A&A 670, A18 (2023)
https://doi.org/10.1051/0004-6361/202243154

Astronomy & Astrophysics

The globular cluster system of the nearest Seyfert II galaxy Circinus

C. Obasi[1,2], M. Gómez[1], D. Minniti[1,3], J. Alonso-García[4,5], M. Hempel[1,9], J. B. Pullen[1], M. D. Gregg[6], L. D. Baravalle[7], M. V. Alonso[7,8], and B. I. Okere[2]

[1] Instituto de Astrofísica, Facultad de Ciencias Exactas, Universidad Andres Bello, Av. Fernandez Concha 700, 7591538 Las Condes, Santiago, Chile
e-mail: c.obasi@uandresbello.edu
[2] Centre for Basic Space Science, University of Nigeria, 410102 Nsukka, Nigeria
[3] Vatican Observatory, 00120 Vatican City State, Italy
[4] Centro de Astronomía (CITEVA), Universidad de Antofagasta, Av. Angamos 601, 1270300 Antofagasta, Chile
[5] Millennium Institute of Astrophysics, Nuncio Monseñor Sotero Sanz 100, Of. 104, Providencia, Santiago, Chile
[6] Department of Physics, University of California, Davis, CA 95616, USA
[7] Instituto de Astronomía Teórica y Experimental (IATE, CONICET-UNC), Laprida 854, X5000BGR Córdoba, Argentina
[8] Observatorio Astronómico de Córdoba, Universidad Nacional de Córdoba, Laprida 854, X5000BGQ Córdoba, Argentina
[9] Max-Planck Institute for Astronomy, Koenigstuhl 17, 69177 Heidelberg, Germany

Received 19 January 2022 / Accepted 7 December 2022

ABSTRACT

Context. The globular cluster (GC) system of Circinus galaxy has not been probed previously partly because of the location of the galaxy at −3.8° Galactic latitude, which suffers severely from interstellar extinction, stellar crowding, and Galactic foreground contamination. However, the deep near-infrared (NIR) photometry by the VISTA Variables in the Via Láctea Extended Survey (VVVX) in combination with the precise astrometry of *Gaia* EDR3 allow us to map GCs in this region.
Aims. Our long-term goal is to study and characterise the distributions of GCs and ultra-compact dwarfs in Circinus galaxy, which is the nearest Seyfert II galaxy. Here we conduct the first pilot search for GCs in this galaxy.
Methods. We used NIR VVVX photometry in combination with *Gaia* EDR3 astrometric features, such as astrometric excess noise and the ratio of the sum of the blue photometer (BP) and red photometer (RP) to the broad G passband (BRexcess), to build the first homogeneous catalogue of GCs in Circinus galaxy. A robust combination of selection criteria allows us to effectively clean interlopers from our sample.
Results We report the detection of ∼70 GC candidates in this galaxy at a 3σ confidence level. They show a bimodal colour distribution with the blue peak at $(G-Ks)_0 = 0.985\pm0.127$ mag with a dispersion of 0.211 ± 0.091 mag and the red peak at $(G-Ks)_0 = 1.625\pm0.177$ mag with a dispersion of 0.482 ± 0.114 mag. A GC specific frequency (S_N) of 1.3 ± 0.2 was derived for the galaxy, and we estimated a total population of 120 ± 40 GCs. Based on the projected radial distribution it appears that Circinus has a different distribution of GC candidates than MW and M 31.
Conclusions. We demonstrate that Circinus galaxy hosts a sizeable number of cluster candidates. This result is the first leap towards understanding the evolution of old stellar clusters in this galaxy.

Key words. galaxies: clusters: general – galaxies: stellar content – galaxies: spiral

1. Introduction

Circinus galaxy or ESO 97-G13 is a nearby spiral galaxy first observed by Freeman et al. (1977) on optical plates. The galaxy is found at J2000 RA = $14^h13^m09^s.906$, Dec = −65°20′20.47″ ($l = 311°.326$, $b = -3°.808$); it is highly obscured and veiled by dust and high foreground stellar density from our Galaxy. The central region presents an interstellar extinction in the V band of $A_V = 3.96$ mag obtained by Schlafly & Finkbeiner (2011). It has a radial velocity of 434.41 km s^{-1} (or a redshift of 0.001448, Meyer et al. 2004) and it is located at about 4 Mpc away from the Milky Way (MW). The spectroscopic observations made by Oliva et al. (1994, 1998) showed an active nucleus confirming that Circinus is a Seyfert II galaxy.

The galaxy has an active core that is strong in X-ray, infrared, and radio emissions (Guo et al. 2019; Yang et al. 2009). Matt et al. (1996) found an X-ray spectrum that is consistent with Compton scattering and fluorescent emission from cold matter illuminated by an obscured active nucleus. The IRAS fluxes of 246 Jy at 60 mm and 314 Jy at 100 mm (Ghosh et al. 1992; Yamada et al. 1993) are consistent with a far-infrared luminosity of $6 \times 10^9\,L_\odot$, which suggest a high level of starburst activity. It has been shown that Circinus contains a bright compact source through radio continuum observations (Freeman et al. 1977; Whiteoak & Bunton 1985; Harnett 1987; Davies et al. 1998) and prominent radio lobes roughly perpendicular to the galaxy's major axis (Harnett et al. 1990; Elmouttie et al. 1995). Marconi et al. (1994) detected a circumnuclear ring in the Hα line, which implies a high concentration of molecular gas (see also Jones et al. 1999; Koribalski et al. 2004). Jones et al. (1999) showed that Circinus galaxy is over 80 arcmin long, or nearly 100 kpc, using its distance of 4 Mpc from HI observations taken with the Australia Telescope Compact Array (ATCA). They also found that Circinus has a large-scale spiral

Table 1. Parameters of Circinus galaxy.

			Reference
Central position	α, δ (J2000)	$14^h13^m10\overset{s}{.}2$, $-65°20'20''$	1
	l, b	$311\overset{\circ}{.}3$, $-3\overset{\circ}{.}8$	1, 3
Type		Sb	1
Distance	D	4.0±0.8 Mpc	1, 2
Optical extent at B_{25}		$6\overset{'}{.}9\times2\overset{'}{.}7$	1
H I extent (**)		$32'\times15'$	2
Position angle	PA_{HI}	210°±5°	2
Inclination angle	i_{HI}	65°±2°	1
Systemic velocity	υ_{sys}	439±2 km s^{-1} (H I)	1
Heliocentric velocity		380±47 km s^{-1} (optical)	1
Velocity width	$\Delta_{\upsilon 20}$	290±10 km s^{-1} (H I)	1
Rotation velocity	υrot	152±7 km s^{-1} (H I)	1
Far-infrared luminosity	LFIR	$6\times10^9\ L_\odot$	1
H I mass	M_{HI}	$7.2\pm0.5\times10^9\ M_\odot$	2
		$9\times10^9\ M_\odot$	3
Total mass	M_{tot}	$1.2\pm0.2\times10^{11}\ M_\odot$	1
Global star formation rate	SFR	$3-8\ M_\odot$ yr^{-1}	3

Notes. (**)The half width of the H I column density distribution after Gaussian correction.
References. [1] Jones et al. (1999); [2] Freeman et al. (1977); [3] For et al. (2012).

pattern with the inner radius being about 250 arcsec or 5 kpc. It contains a highly elongated structure with non-circular motions, which suggests that Circinus is a barred spiral galaxy. Low-resolution 21 cm observations have revealed the enormous HI envelope of the galaxy; its large-scale gas disc is shown to extend over an area more than one degree in diameter and is argued to be much larger than the stellar disc. The HI physical diameter of Circinus resembles that of the M 83 galaxy (Jerjen & Koribalski 2008).

Circinus appears to be isolated and has no known merger history. For et al. (2012) presented a detailed study of the galaxy, investigating its star formation, and dust and gas properties in both the inner and outer disc using high-resolution *Spitzer* mid-infrared images with IRAC (3.6, 5.8, 4.5, 8.0 μm) and MIPS (24 and 70 μm) and sensitive HI data from the ATCA and the 64 m Parkes telescope. They derived $A_V = 2.1$ mag from the spectral distribution and showed global star formation rates between 3 and 8 $M_\odot$ yr^{-1}. Together with Centaurus A they are the closest active galaxies to the MW. We show in Table 1 the measured parameters of this galaxy. Despite all the richness and interesting features found in this galaxy, most studies have been limited to its nuclear region because of the location in the sky. The 2MASS Large Galaxy Atlas (Jarrett et al. 2003) gave us the initial view of the stellar content of Circinus, which was limited by its dust opacity at 2 μm and its dense stellar foreground, which prevented a detailed investigation of its large-scale structure and star clusters. To date, we still do not understand how the old stellar associations of Circinus are distributed.

Star clusters are crucial to our understanding of the evolution of galaxies. For this reason we are using a combination of VISTA Variables in the Vía Láctea Extended Survey (VVVX Minniti 2018) data with *Gaia* EDR3 (Gaia Collaboration 2021) to conduct the first search of globular clusters (GCs) in Circinus galaxy. The paper is organised as follows. In Sect. 2 we describe the observations, and in Sect. 3 we elaborate on the methods we used to search for the GCs. We present our results in Sect. 4, and the summary and our conclusions in Sect. 5.

2. Observations

We used the VVVX described by Minniti (2018) and Obasi et al. (2021), which maps the Galactic bulge and southern disc in the near-infrared (NIR) with the VISTA InfraRed CAMera (VIRCAM) at the 4.1 m wide-field Visible and Infrared Survey Telescope for Astronomy (VISTA; Emerson & Sutherland 2010) at the European Southern Observatory (ESO) Paranal Observatory (Chile). In this work, the data used consist of the two VVVX tiles e656 and e657, which cover the field of Circinus galaxy. We created a photometric catalogue using SExtractor version 2.3.1 (Bertin & Arnouts 1996), which is a program designed to detect, deblend, measure, and classify sources from astronomical images. SExtractor is known as a useful tool for analysing overlapping objects found within the crowded region of the bulge and the disc. In order to generate the catalogue we used SExtractor in double-image mode with the K_s image (full width at half maximum, $FWHM = 0.5''$) as a reference because of its better quality. The K_s image was used for source detection, and H and J passband images were used for colour measurements only. We set our DETECT_THRESH and ANALYSIS_THRESH to 5σ in order to minimise spurious detections.

The photometry in each of the VVVX fields e656 and e657 was treated independently. The magnitudes were corrected for total interstellar extinctions following the maps of Schlafly & Finkbeiner (2011). Based on our detected point sources, we show in Fig. 1 the total interstellar extinction distribution in the two VVVX fields which include Circinus galaxy. The peak in A_V is around 1.7 mag with a mean value of ∼2 mag. The complex pattern shown by the interstellar extinction makes it necessary to perform this correction locally instead of adopting a global A_V. Using $A_V = 3.1 \times E(B-V)$, we derived $A_V = 3.96$ mag for Circinus centre. Relative extinctions $A_J = 0.280\times A_V$, $A_H = 0.184\times A_V$, and $A_{Ks} = 0.118\times A_V$ from Catelan et al. (2011) were used to obtain interestellar extinctions for each point sources. Once the catalogues were generated for each field, we used the point spread function (PSF)

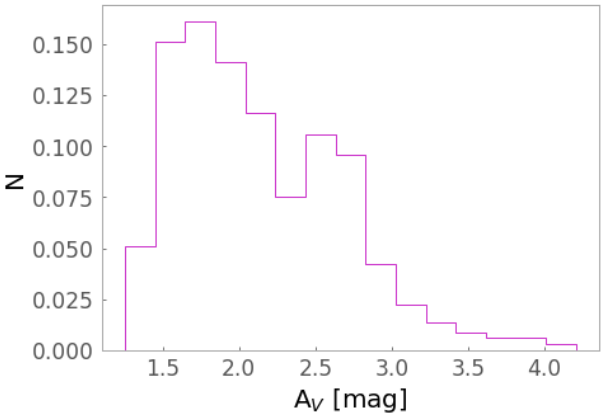

Fig. 1. Total interstellar extinction distribution, A_V mag, derived from the maps of Schlafly & Finkbeiner (2011) of all point sources detected in the two studied VVVX tiles within Circinus galaxy.

photometry to calibrate them using a preliminary version of the new VVVX photometric catalogue (Alonso-García et al., in prep.; hereafter AG22). Before the calibration, the mean differences between AG22 and our instrumental magnitudes from SExtractor (MAG_AUTO) for the J, H, and K_s passbands are 0.091, 0.088, and 0.053 mag, respectively. In Fig. 2, we show the differences in the J, H, and K_s magnitudes compared with our magnitudes after the zero point (upper panels) and colour (bottom panels) corrections. For the upper panels, we divided our photometry into 1 mag bins and computed the median difference for each bin. For the bottom panels, bins of 0.4 mag were used and the median values for the differences in $JHKs$ were also computed. The median values were then plotted; there seems to be no clear colour dependence. Our detection limits in J, H, and K_s passbands were 18.5, 18.0, and 17.5 mag, respectively. At the completion of the calibration, the two fields were concatenated as a single catalogue. As there was a small superposition between the two VVVX fields, duplicate sources were removed and a sample of homogeneous data for Circinus galaxy was generated.

3. Searching for globular clusters

First, detected objects were classified into point and extended sources using the CLASS_STAR index provided by SExtractor. CLASS_STAR is a stellarity index that is associated with the light distribution of the source. It ranges from 1 for point sources, such as stars, to 0 for extended objects, such as galaxies. To distinguish between the different source types, SExtractor relies on a multi-layer feed-forward neural network trained using supervised learning to estimate a posteriori the probability that the detection would be either a point source or an extended object. We selected point sources by adopting CLASS_STAR $\geq$0.5. A total of 902 667 objects passed this selection, which represents about 80% of all source detected. We then applied colour cuts in order to photometrically select those points sources that have colours and magnitudes consistent with those expected for GCs in other galaxies. From the catalogue of Wang et al. (2014) there are 568 spectroscopically confirmed GCs (Galleti et al. 2004)[1] that we used for our colour selection. Our adopted colour cuts were restricted to $\pm 2\sigma$ statistical level from the mean GC colours. This allowed us to minimise the contamination from foreground stars. In Fig. A.1 we show the complete Wang et al. (2014) GC catalogue in blue and in magenta the confirmed GCs. The mean colour obtained and their limits as applied to our selection are given as 0.655, $0.113 \leq (J-H)_0 \leq 1.197$ mag; 0.189, $-0.424 \leq (H-K_s)_0 \leq 0.802$ mag; and 0.839, $0.159 \leq (J-K_s)_0 \leq 1.519$ mag. We obtained 791 662 sources after the colour cuts, which accounts for 87.7% of the total sources. The colour–colour selected region used for the rest of the analysis is shown in Fig. 3. The upper panels show our selected region with black points and the lower panels our selection overlaid with confirmed GCs of M 31 (Wang et al. 2014), M 81 (Nantais & Huchra 2010), and NGC 5128 (Woodley et al. 2009; Taylor et al. 2015). They indicate that GCs occupy a wide range of colours.

Additionally, the sources that satisfy our colour cuts were cross-matched with *Gaia* EDR3 within a radius of 0.5″. *Gaia* is an all-sky astrometric catalogue of more than a billion sources. The spatial resolution of the survey has improved from 0.40″ in *Gaia* DR2 (Lindegren et al. 2018) to 0.18″ in *Gaia* EDR3 (Gaia Collaboration 2021), where the GCs have effective radii of ∼2−10 pc, as given in Harris (1991). At the distance of Circinus, they appear as marginally extended sources to *Gaia*, which has a resolution of 0.059″ per pixel in the scanning direction. By combining the VVVX data with a pixel size of 0.34″ and *Gaia* EDR3 data, we can take advantage of some of the *Gaia* astrometric features to resolve the GCs of Circinus galaxy. The *Gaia* EDR3 catalogue for a circular region of radius 1.6 deg. centred on RA = 213.29° and Dec = −65.33° (corresponding to a diameter of 108 kpc at the distance of Circinus) was downloaded. At low Galactic latitudes the contamination by foreground stars is very severe (Baravalle et al. 2018). Because Circinus is located at $b = -3.8°$, just below the Galactic plane, and also veiled by the Galactic disc, most of the detected objects are therefore expected to be stars within the Galactic plane. The use of *Gaia* EDR3 is crucial in eliminating MW foreground stars using their proper motions and parallaxes. Any source with a significant proper motion or parallax can be excluded from our analysis as being a foreground object. The total proper motion of each object was obtained assuming that the combined proper motion has a χ^2 distribution with two degrees of freedom. In this way, the proper motion likelihood of one cumulative distribution function (CDF) of the Rayleigh distribution was assigned to each object. In this study we only considered objects whose proper motion probability values are consistent with zero at 2σ. Sources with probability values smaller than −1 or greater than 1 are considered to be foreground stars, were assigned proper motion likelihood = 0, and were therefore removed from our analysis.

A similar procedure was adopted for the parallax. We assumed that the measurements follow a Gaussian distribution. If the parallax is significant at 2σ, the likelihood assigned is $-0.4 \leq \mathrm{Plx} \leq 0.4$ Sources with $>3\sigma$ parallax measurements were assigned parallax likelihood = 0 and were not considered in the rest of our analysis. As the fourth step, the sources that satisfied our previous criteria were then subjected to some tests with the astrometric excess noise (AEN) and phot_bp_rp excess factor (BRexcess). These are two *Gaia* parameters found to be very useful in disentangling point and extended sources. Voggel et al. (2020) demonstrated how these two parameters might be used to select extended sources such as GCs out to a distance of 25 Mpc. The AEN is a statistical computation that quantifies the goodness of the fit of their five-parameter astrometric model to the astrometry for each target. The AEN is measured in

[1] This is the 2012 revised and updated Bologna catalogue of M 31 GCs and candidates. It contains 625 confirmed GCs, 568 of which have a match in the Wang et al. (2014) catalogue.
https://cdsarc.cds.unistra.fr/viz-bin/cat/V/143

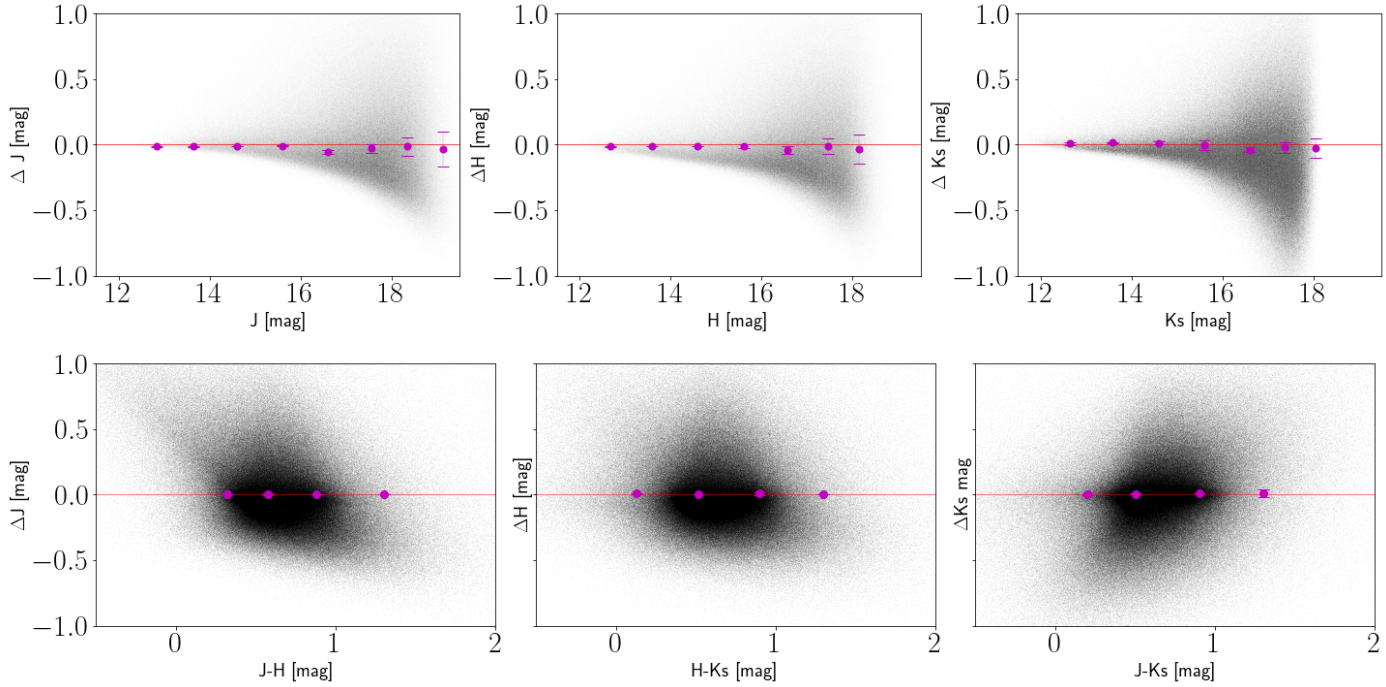

Fig. 2. Differences in J, H, K_s as a function of magnitude (*upper panels*) and colour (*bottom panels*) compared to AG22. The median values of each magnitude and colour bin are shown, as well as their associated errors (in magenta).

milliarcseconds (mas) and is equal to 0 for a well-fit star and larger for a poorer fit. It has been shown in Voggel et al. (2020) that objects that are extended sources generally have larger AEN values and this could be exploited in selecting marginally resolved objects such as GCs. On the other hand, the BRexcess gives the ratio of the sum of the fluxes of the blue photometer (BP, 3300−6800 Å) and red photometer (RP, 6400−10 500 Å) to the flux in the broad-G passband. Its importance and usefulness come from the unique way these fluxes are derived. Both the BP and RP magnitudes are measured from the flux within a larger aperture of 3.4×2.1 arcsec^2, while the G magnitude is obtained from profile fitting with an effective resolution of 0.4″ (Evans et al. 2018). The variation means that extended sources have a higher BRexcess than point sources since fitting an effective point-source profile to an extended source in the G passband misses some of the total light. Voggel et al. (2020) used the combination of these two parameters to identify over 600 new luminous cluster candidates in the halo of NGC 5128 out to a projected radius of 150 kpc. In a follow-up study by Hughes et al. (2021), they used this method to estimate a total population of 1450±160 GCs to a projected radius of 150 kpc in NGC 5128 demonstrating its robustness. In using both the AEN and BRexcess, they calculated the likelihood that a source is an extended source (GC) within a radial range of 10−60′ from the galaxy centre to define a line of 3σ above the mean foreground star; the AEN and BR derived values are given in Eqs. (1) and (2):

$$\mathrm{AEN}_{3\sigma} = 0.297 + 5.63 \times 10^{-8}\, e^{0.895G}, \quad (1)$$

$$\mathrm{BRexcess}_{3\sigma} = 1.26 + 2.79 \times 10^{-8}\, e^{0.853G}. \quad (2)$$

We tested the above procedure by using spectroscopically confirmed GCs in M 81 of Nantais & Huchra (2010) and NGC 5128 of Woodley et al. (2009) and Taylor et al. (2015). The M 81 catalogue comprises 108 confirmed GCs; after cross-matching with the *Gaia* EDR3 catalogue, we found 77 counterparts. We adopted a distance modulus of 27.64±0.09 for M 81 (Freedman & Madore 1988) and corrected for relative extinctions in G passband with the relation $A_G = 0.86 \times A_V$ given by Fernández-Alvar et al. (2021). For each source the distance to the centre was computed, and six sources had distances greater than 10 kpc from the galaxy centre. For NGC 5128 we used two spectroscopically confirmed catalogues comprising 37 GCs by Woodley et al. (2009) and 140 GCs by Taylor et al. (2015). These catalogues were then cross-matched with *Gaia* EDR3, and 134 sources were found in common. For NGC 5128 a distance modulus of 27.9±0.2 was adopted from Rejkuba (2004). Then we proceeded to compute the distance of each GC from the centre and a total of 31 sources were found to have radial distances greater than 10 kpc. Figure 4 shows the properties for NGC 5128 and M 81 using Eqs. (1) and (2) of Hughes et al. (2021) as AEN versus G magnitudes and BRexcess versus G magnitudes (upper and lower panels, respectively). Blue points are sources with radial distances of less than 10 kpc, while black points are sources with distances greater than 10 kpc. The red curve represents the 3σ probability that a source is more extended than a point source (in our case GCs). We find the brighter objects tend to have smaller AEN values, which could be attributed to the statistical uncertainties in *Gaia* observations. We might conclude that all the black points are consistent with being point sources for NGC 5128. Three points are below the curve for M 81 and they might be misclassified, most probably as foreground stars (see Hughes et al. 2021). It is important to note that the above procedure is sensitive to objects with distances greater than 10 kpc to the galaxy centre. In this analysis we only considered the outermost parts of the galaxy, where the internal extinction is less severe compared to the central part. We applied this procedure to all the sources in Circinus galaxy that satisfied our previous criteria. There are 260 sources that satisfied the AEN criterion and 176 sources after the BRexcess cut. As an additional step, the sources should also satisfy the spread model parameter criterion, Φ, which is another star-galaxy

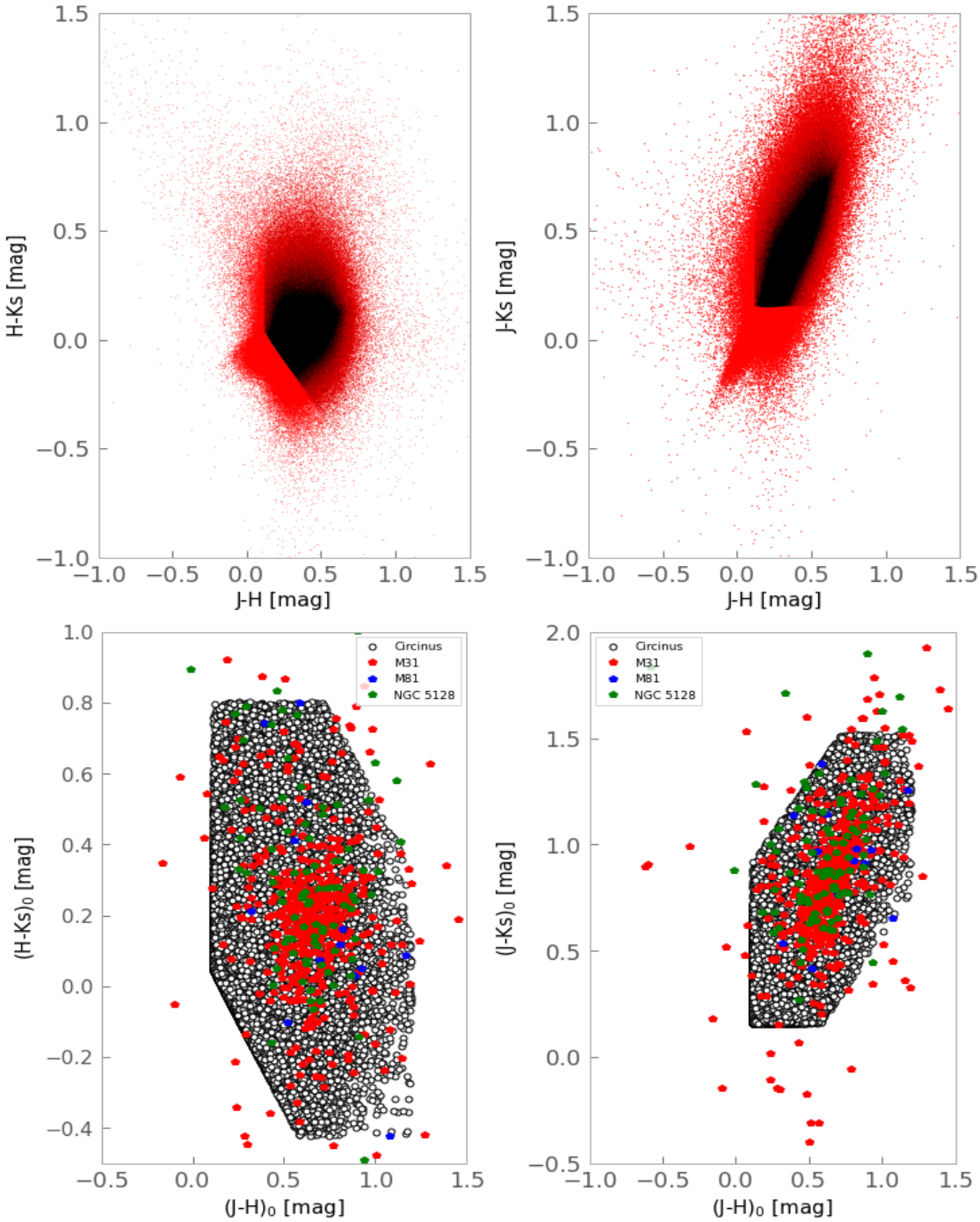

Fig. 3. Colour–colour diagrams $H - K_s$ vs $J - H$ and $J - K_s$ vs $J - H$ (*upper panels*) showing the colour cuts used for the analysis (in black). The *lower panels* reproduce the same region, but overplotted with GCs from M 31 (Wang et al. 2014), M 81 (Nantais & Huchra 2010), and NGC 5128 (Woodley et al. 2009; Taylor et al. 2015).

classifier that was added in the newest SExtractor versions. The value of this parameter is usually zero for stars, positive for extended sources and negative for detections smaller than the PSF, such as cosmic rays. We adopted the same cut used by Baravalle et al. (2018) to search for extragalactic sources in the VVV data ($\Phi > 0.002$). For Circinus galaxy, 141 of the sources satisfy all the above criteria.

Finally, we also examined the ellipticity and FWHM of the sources inspecting their morphology (roundness and size) as one critical criterion for selecting GCs (see Minniti et al. 1996; Alonso & Minniti 1997; Rejkuba 2001). Both features are convenient parameters to obtain a bona fide GC sample. However, using only FWHM as the discriminating criterion leads to the rejection of both very concentrated and very loose clusters. Conversely, using only roundness underestimates the GC sample. By applying these two stringent criteria together, we can trade off the masquerading interlopers against some true genuine GCs. We adopted $\varepsilon \leq 0.4$ consistent with Georgiev et al. (2009) and Woodley & Gómez (2010) and $2 \leq FWHM$ (pixels) ≤ 4 consistent with Alonso & Minniti (1997), Rejkuba (2001), and obtaining a final sample of 78 potential Circinus GCs within the colour limits.

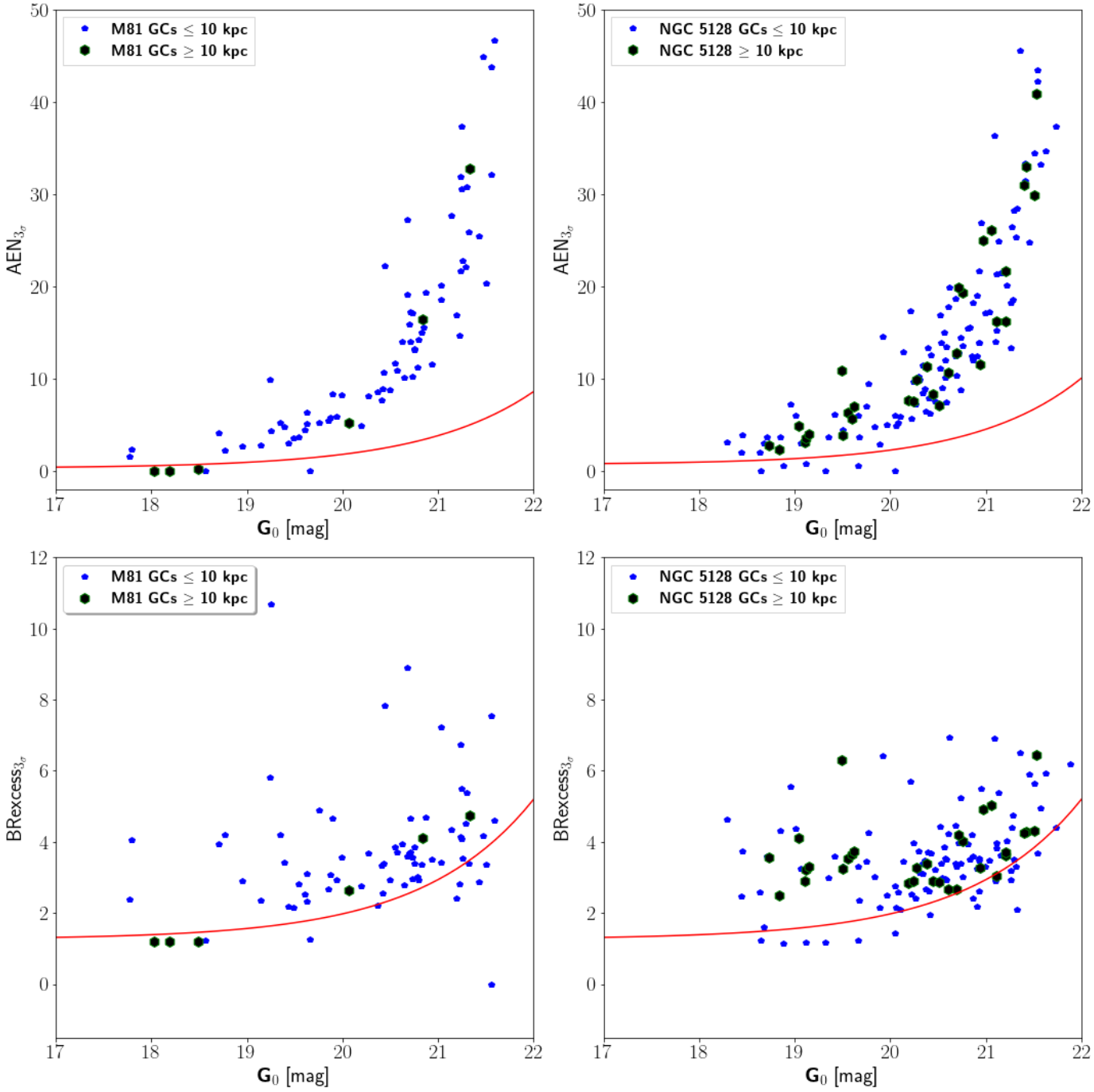

Fig. 4. Spectroscopically confirmed GCs in M 81 (Nantais & Huchra 2010) and NGC 5128 (Woodley et al. 2009) combined with Taylor et al. (2015) and *Gaia* catalogues. The AENs and BRexcess as a function of the G magnitudes are shown in the *upper and bottom panels*, respectively. Blue points represent GCs at ≤10 kpc from the galaxy centre while black points, those GCs at ≥10 kpc. The red curve defines 3σ above the mean foreground stars.

In Fig. 5 we show the AEN as a function of G magnitudes with Eq. (1), (left panel) and BRexcess as a function of G magnitudes together with Eq. (2), (right panel) for the 902 667 points in Circinus galaxy. Overplotted in blue are our final GC candidates.

4. Results

Our final sample is composed of 78 GC candidates (including contaminators) found in Circinus galaxy. We corrected for interstellar extinction in each of the objects. Figure 6 shows the $(G-K_s)_0$ versus K_s colour-magnitude diagram, and the $(G-K_s)_0$ versus $(8545\,J-K_s)_0$ and $(G-K_s)_0$ versus $(H-K_s)_0$ colour–colour diagrams (left, middle, and right panels). In Fig. 7 we show the NIR luminosity function (M_{Ks}) of the 78 GCs compared with those of the MW (Nantais et al. 2006) and M 31 (Wang et al. 2014). The MW sample contains 99 GCs, while M 31 have 568 confirmed GCs. The figure shows that we are only detecting the brightest GCs in Circinus. Our sample did not reach the expected GCs turnover in infrared of $M_{Ks} = -10$ mag. If we assume a $(V-K_s)$ mean colour of 2.5 mag, it is difficult to accurately estimate the total number of GCs (N_{GC}) in Circinus and their specific frequency (S_N), which defines N_{GC} per unit

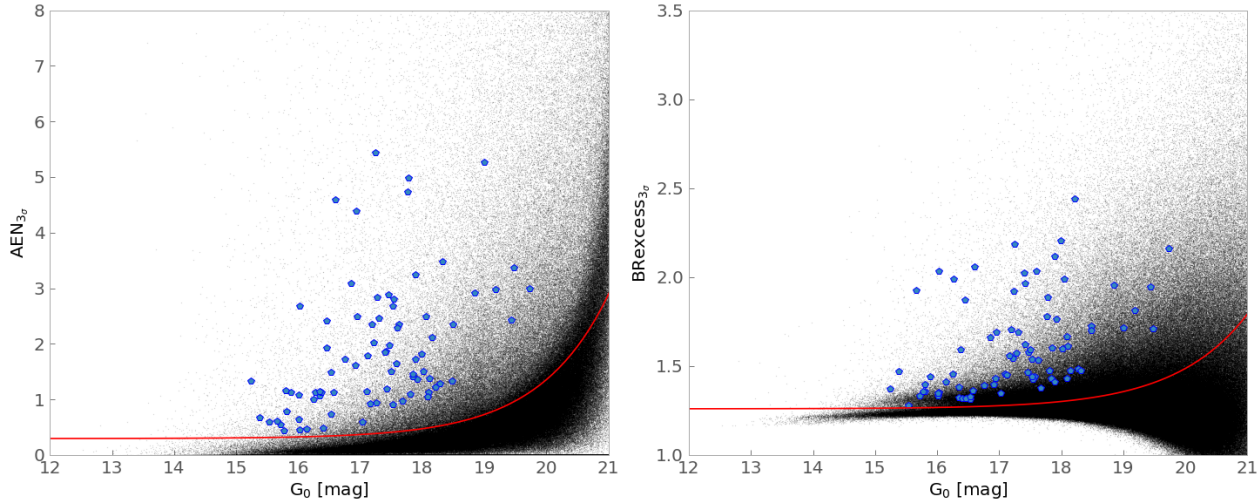

Fig. 5. AENs and BRexcess as a function of the G magnitudes (*left and right panels*, respectively). The point sources are over-plotted with our final sample in blue. The red curves show the 3σ criteria derived by Hughes et al. (2021) to select GCs in NGC 5128.

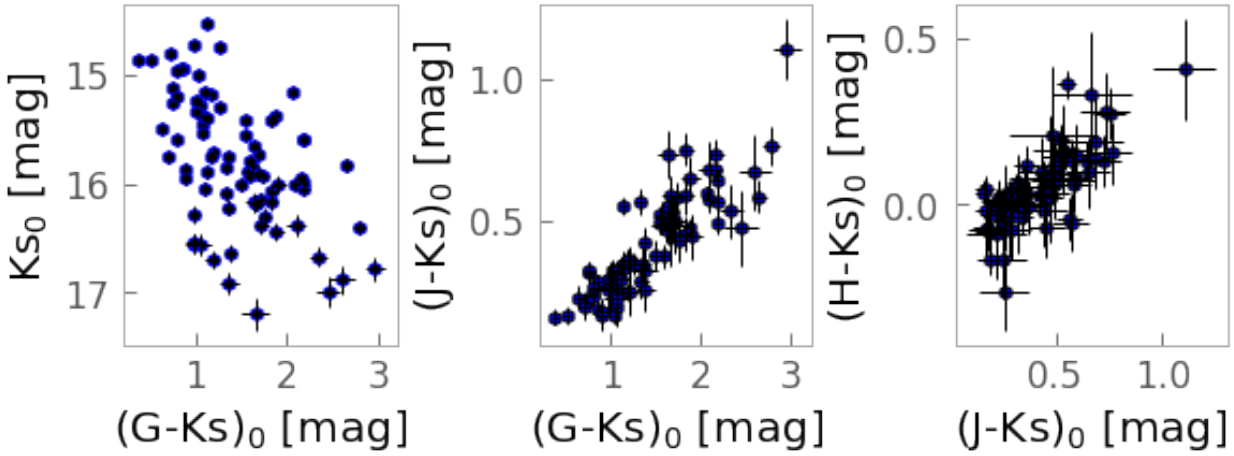

Fig. 6. NIR–optical colour–magnitude diagram (*left panel*), NIR–optical colour–colour diagram (*middle panel*), and NIR colour–colour diagram (*right panel*) for the GC candidates in Circinus galaxy.

galaxy luminosity normalised to a galaxy with an absolute V magnitude of -15 (Harris & van den Bergh 1981). However, we can use the relation given in Harris et al. (2013) to roughly estimate $N_{\rm GC}$. The relation reads

$$N_{\rm GC} = (300 \pm 35)\left[\left(\frac{R_{\rm e}}{10\,{\rm kpc}}\right)\left(\frac{\sigma_{\rm e}}{100\,{\rm km\,s^{-1}}}\right)\right]^{1.29\pm0.03}, \quad (3)$$

where $R_{\rm e}$ is the effective radius of the galaxy and $\sigma_{\rm e}$ is the velocity dispersion. The above parameters for Circinus have been reported, where $R_{\rm e}$ = 6.5 kpc±1 kpc Jarrett et al. (2003) and $\sigma_{\rm e} = 75\pm20\,{\rm km\,s^{-1}}$ Hu (2008). The total number of GCs in Circinus is therefore estimated to be 120±40. With this result we can calculate the S_N of GCs using the equation provided in Harris & van den Bergh (1981) represented by

$$S_N = N_{\rm GC} 10^{0.4(M_V^{\rm T}+15)}, \quad (4)$$

where $M_V^{\rm T}$ is the absolute visual magnitude. Given that the apparent magnitude is 12.1 mag (De Vaucouleurs et al. 1991) and A_V = 3.96 mag, this implies that the absolute magnitude M_V = −19.87 mag; we obtained a S_N of 1.3±0.24. This result is consistent with S_N values for spiral galaxies usually ≤1 (van den Bergh & Harris 1982).

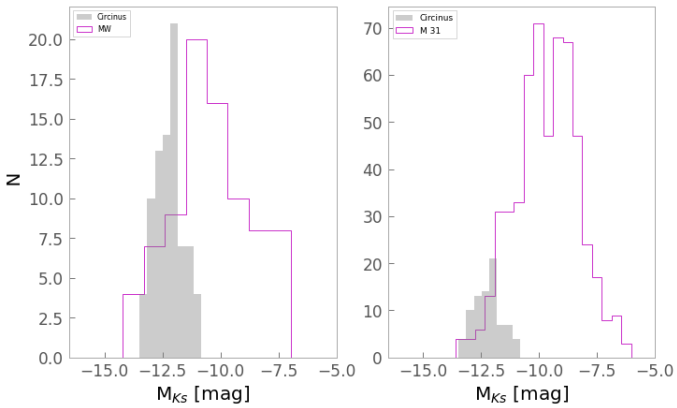

Fig. 7. Luminosity function of Circinus GC candidates in the K_s passband together with that of the MW (Nantais et al. 2006) and M 31 (Wang et al. 2014; *from left to right*).

We tested for bimodality in the colour distribution of our sample. Most GCs found in massive galaxies have shown to exhibit bimodal colour distributions (see Brodie & Strader 2006; Brodie et al. 2014; Harris et al. 2017). Nonetheless, in some

Table 2. GMM test results.

Colour	N	Blue	Red	$f_{\rm blue}$	$f_{\rm red}$	Kurt	DD	$p(\chi^2)$
$(G-J)_0$	78	0.964±0.125	1.950±0.337	56.8±19.3	21.2±19.3	0.594	3.17±1.17	0.037
$(G-H)_0$	78	1.095±0.172	1.771±0.315	47.5±22.0	30.5±22.0	0.339	2.58±0.92	0.285
$(G-K_s)_0$	78	0.985±0.127	1.625±0.308	33.8±16.4	44.2±16.4	0.308	2.08±0.69	0.039

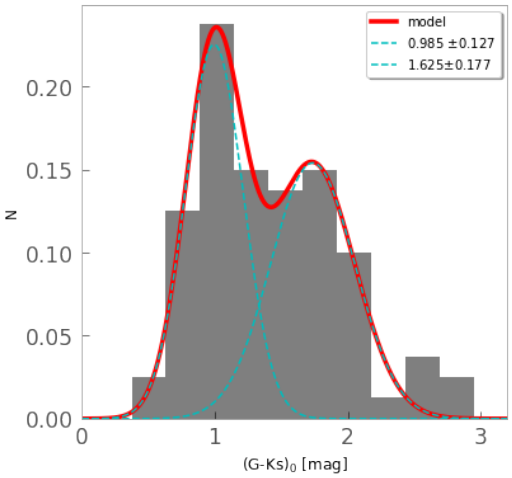

Fig. 8. $(G-Ks)_0$ colour distribution of our GC candidates.

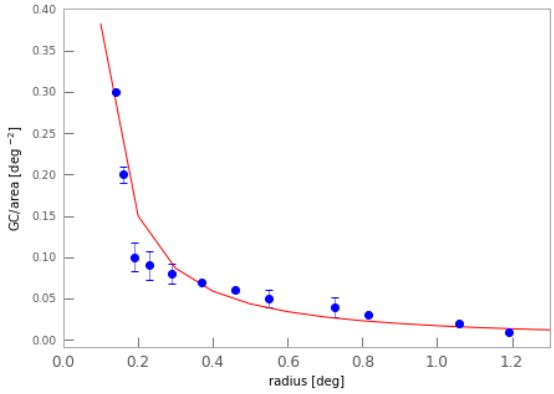

Fig. 9. Surface density profile of our GC candidates in radial bins. The surface density follows a power-law distribution with $\rho_{\rm GC} \propto r^{-1.4}$ represented by the red solid curve.

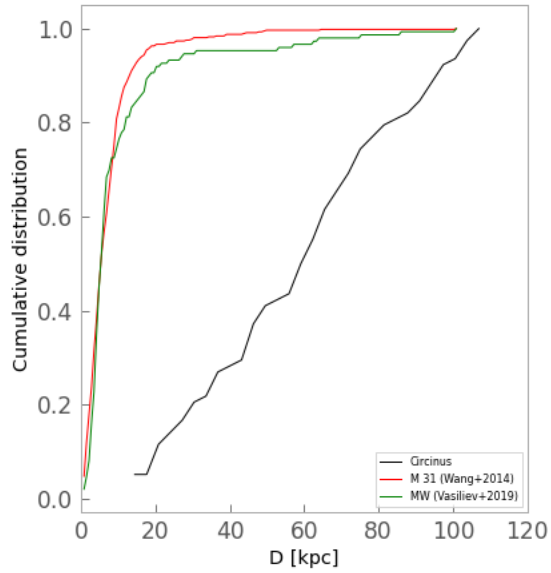

Fig. 10. Cumulative distribution of GCs with increasing galactocentric distance D for Circinus, M 31, and the MW (in black, red, and green, respectively).

studies (Gebhardt & Kissler-Patig 1999; Chies-Santos et al. 2012; Beasley et al. 2018) there have been reports of unimodal colour distributions for GCs, which were argued to have formed at the same time in isolated galaxies with no history of mergers. We used the Gaussian mixture model (GMM) developed by Muratov & Gnedin (2010) specifically to test for bimodality in GC systems. The model shows that our sample is nicely described by a bimodal distribution with the blue peak at $(G-K_s)_0 = 0.985\pm0.127$ mag with a dispersion of 0.211 ± 0.091 mag and the red peak at $(G-K_s)_0 = 1.625\pm0.0177$ mag with a dispersion of 0.482 ± 0.114 mag[2].

A similar bimodal distribution can also be observed in other colour combinations; in Table 2 we present the results of the GMM analysis for the colours $(G-J)_0$, $(G-H)_0$, and $(G-Ks)_0$. In column one we present the colour, in Col. 2 the number of objects, in Cols. 3 and 4 the blue and red peaks, in Cols. 5 and 6 we provide the fraction of objects in each peak, and in Cols. 7–9, we show the Kurtosis, the peak separations (measured in units of the fitted σ_s for the two Gaussian models), and the $P(\chi^2)$ values. Two of the three colours that have been inspected show consistency between the blue and red fractions in the colour distribution. The third colour has a bias favouring the red fraction. Nevertheless, the low $P(\chi^2)$ values from the GMM tests confirm that a bimodal Gaussian distribution is preferred to a unimodal distribution. Figure 8 shows this colour distribution of GC candidates with a bin size of 0.1 mag, giving more evidence of their nature. The red curve shows the fit.

[2] The GMM code employs the likelihood-ratio test to compare the goodness of fit for a double Gaussian vs a single Gaussian. It estimates the probability of a best-fit double model providing the means,widths of the two components, their separation DD in terms of combined widths, and their overall kurtosis. Importantly, GMM also provides the positions, relative widths, and fraction of objects associated with each peak, as well as their uncertainties based on bootstrap resampling.

The density distribution also follows a power law, which is frequently observed for GCs with $\rho_{\rm GC} \propto r^{-1.4}$. The number of GCs is still too uncertain to determine a proper radial profile. However, it is clear from Fig. 9 that our cluster candidates follow a distribution that closely resembles many other extragalactic GC systems (see e.g. Gómez & Richtler 2004; Brodie & Strader 2006). Even if the true profile and background level remains to be determined, a clear concentration in the central parts of Circinus can be seen, which favours a true GC nature of our sample.

In Fig. 10 we compare the projected radial distances of Circinus, M 31, and MW GCs. As can be observed, large

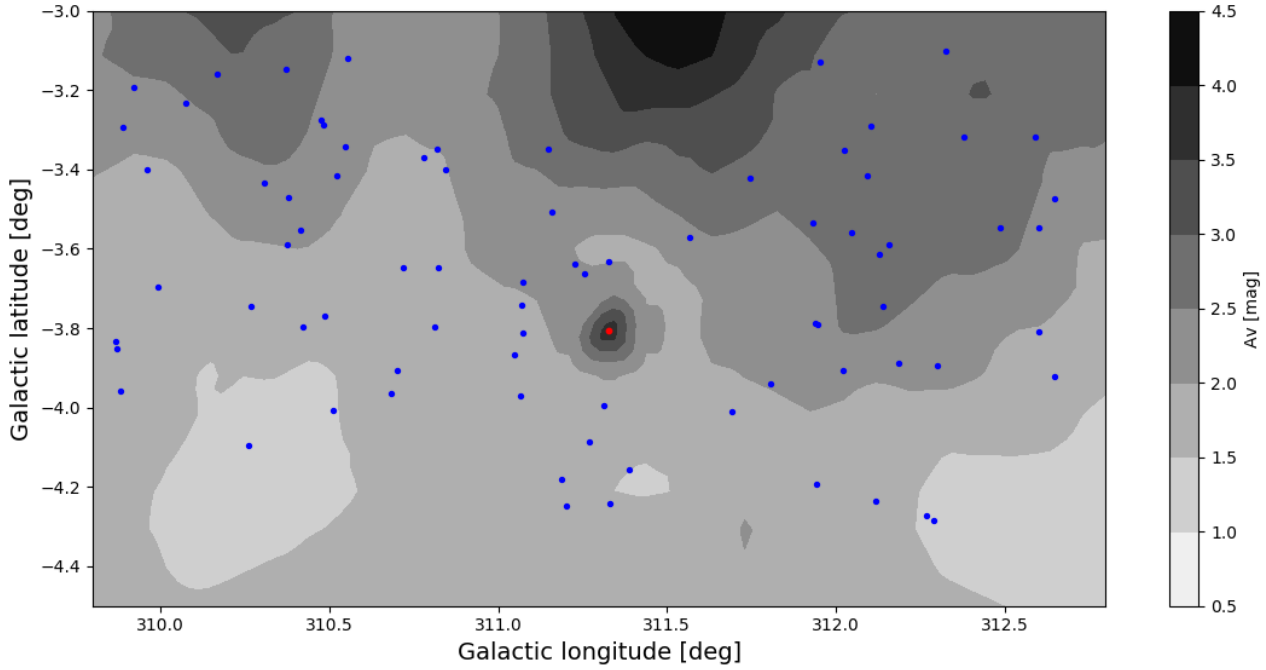

Fig. 11. Spatial distribution of the 78 GC candidates in Circinus galaxy. The candidates are represented with blue points. The red dot indicates the adopted centre of Circinus. The total optical A_V insterstellar extinctions from the maps of Schlafly & Finkbeiner (2011) are shown in greyscale (see colour bar at right).

concentrations of clusters are found for $D < 30$ kpc in M 31 and MW. We used the 568 confirmed GCs in M 31 (Wang et al. 2014) and 150 in the MW catalogue (Vasiliev 2019) for this comparison, of which 93.3% and 81.3% are within distances $\lesssim$30 kpc compared to 12.5% for Circinus. In the light of these findings, a fundamental question arises regarding the level of contamination in our sample, and regarding the similarity in GC distributions between MW, M 31, and Circinus. As part of our effort to provide some insight into this question, we examined two empty fields at opposite ends of Circinus that were about 2.4° away from Circinus. The fields are located at similar latitudes, and their extinction patterns are similar to those of Circinus with a mean $A_V \sim 2$ mag. The area covered is the same by construction. We applied the same procedure that we used for analysing Circinus. In each of the fields we found eight and ten sources that met our adopted criteria. This amounts to 10.3% and 12.8% contamination, respectively. Therefore, we estimate that our sample is contaminated with 11.5% interlopers. Based on the projected radial distribution it appears that Circinus has a different distribution of GC candidates than MW and M 31. However, the data available at present do not allow a conclusive assessment of the differences in GC radial distribution. Our sample must be cleaned up to eliminate interlopers, and GCs must be searched for in the bulge and disc to get a good idea of the overall distribution before such a claim can be made. Follow-up spectroscopic observations of these candidates will help to weed out contaminators. The ratio of our 70 GC candidates (interlopers accounted for) to the estimated 120±40 GC population expected in Circinus suggests that about 58% of the total GC population is located in the halo. In Fig. 11 we show the spatial distribution of the 78 selected GC candidates in Galactic coordinates. The regions with the same optical total interstellar extinction A_V derived from the extinction maps of Schlafly & Finkbeiner (2011) are superimposed with different A_V levels, as shown by the greyscale bar. The closest object to the galaxy centre is located at a projected radial distance of about 11 kpc. About 80% of the cluster candidates are located in regions with low A_V interestellar extinctions (0.5 to 2.0 mag). However, more GC candidates might be missing at central regions with higher extinctions. Table A.1 shows the 78 GC candidates, listing the identification in Col. (1); the J2000 equatorial coordinates in Cols. (2) and (3); the J_0, H_0, and K_{s_0} magnitudes with their respective errors in Cols. (4)–(9); the *Gaia* magnitude in Col. (10); the FWHM in Col. (11); the ellipticity and the A_V, A_J, A_H, A_{Ks}, A_G extinctions in Cols. (12)–(17); and the galactocentric distances in Col. (18).

5. Conclusions

This is the first study of the old stellar association in Circinus galaxy, which is the nearest known Seyfert II galaxy. We performed our search using VVVX photometry together with the *Gaia* EDR3 catalogue. Taking advantage of the sharp contrast and reduced reddening sensitivity in the NIR VVVX frames and the excellent resolution of the *Gaia* EDR3 astrometry features (AEN and BRexcess), we found a total of 78 GC candidates that satisfied all our stringent criteria. The GC colour distribution is well described by two normal functions with a blue peak at $(G - Ks)_0 = 0.985\pm0.127$ mag with a dispersion 0.211 ± 0.091 mag and a red peak at $(G-Ks)_0 = 1.625\pm0.177$ mag with a dispersion of 0.482 ± 0.114 mag. We estimated $N_{\rm GCs}$ of 120±40 and derived a S_N of 1.3±0.2. The density distribution follows a power law with $\rho_{\rm GC} \propto r^{-1.4}$. The most distant GCs that we detected are located at a projected distance of about 107 kpc from the centre of the galaxy, indicating that Circinus has an extended GC system. The true nature of these objects must be determined through follow-up spectroscopic observations.

Acknowledgements. We gratefully acknowledge the use of data from the ESO Public Survey program IDs 179.B-2002 and 198.B-2004 taken with the VISTA telescope and data products from the Cambridge Astronomical Survey Unit. This work has made use of data from the European Space Agency (ESA) mission *Gaia* (https://www.cosmos.esa.int/gaia), processed by the *Gaia*

Data Processing and Analysis Consortium (DPAC, https://www.cosmos.esa.int/web/gaia/dpac/consortium). Funding for the DPAC has been provided by national institutions, in particular the institutions participating in the *Gaia* Multilateral Agreement. We also acknowledge the comments of the anonymous reviewer whose positive feedback helped to improve the quality of this paper. D.M. gratefully acknowledges support by the ANID BASAL projects ACE210002 and FB210003. D.M. and M.G. also gratefully acknowledge support by Fondecyt Project No. 1220724. J.A.-G. acknowledges support from Fondecyt Regular 1201490 and from ANID – Millennium Science Initiative Program – ICN12_009 awarded to the Millennium Institute of Astrophysics MAS.

References

Alonso, M. V., & Minniti, D. 1997, ApJS, 109, 397
Baravalle, L. D., Alonso, M. V., Castellón, J. L. N., et al. 2018, AJ, 155, 46
Beasley, M. A., Trujillo, I., Leaman, R., & Montes, M. 2018, Nature, 555, 483
Bertin, E., & Arnouts, S. 1996, A&A, 117, 393
Brodie, J. P., & Strader, J. 2006, ARA&A, 44, 193
Brodie, J. P., Romanowsky, A. J., Strader, J., et al. 2014, AJ, 796, 52
Catelan, M., Minniti, D., Lucas, P., et al. 2011, RR Lyrae Stars, Metal-Poor Stars, and the Galaxy (Pasadena: The Carnegie Institution of Washington)
Chies-Santos, A., Larsen, S., Cantiello, M., et al. 2012, A&A, 539, A54
Davies, R. I., Forbes, D. A., Ryder, S., et al. 1998, MNRAS, 293, 189
De Vaucouleurs, G., De Vaucouleurs, A., Corwin, H., Jr., et al. 1991, Sky and Telescope, 82, 621
Elmouttie, E., Haynes, R., Jones, K., et al. 1995, MNRAS, 275, L53
Emerson, J., & Sutherland, W. 2010, The Messenger, 139, 2
Evans, D., Riello, M., De Angeli, F., et al. 2018, A&A, 616, A4
Fernández-Alvar, E., Kordopatis, G., Hill, V., et al. 2021, MNRAS, 508, 1509
For, B.-Q., Koribalski, B., & Jarrett, T. 2012, MNRAS, 425, 1934
Freedman, W. L., & Madore, B. F. 1988, AJ, 332, L63
Freeman, K., Karlsson, B., Lynga, G., et al. 1977, A&A, 55, 445
Gaia Collaboration (Brown, A. G. A., et al.) 2021, A&A, 649, A1
Galleti, S., Federici, L., Bellazzini, M., Pecci, F. F., & Macrina, S. 2004, A&A, 416, 917
Gebhardt, K., & Kissler-Patig, M. 1999, AJ, 118, 1526
Georgiev, I. Y., Puzia, T. H., Hilker, M., & Goudfrooij, P. 2009, MNRAS, 392, 879
Ghosh, S., Bisht, R., Iyengar, K., et al. 1992, ApJ, 391, 111
Gómez, M., & Richtler, T. 2004, A&A, 415, 499
Guo, X.-L., Xin, Y.-L., Liao, N.-H., & Fan, Y.-Z. 2019, ApJ, 885, 117
Harnett, J. 1987, MNRAS, 227, 887
Harnett, J., Whiteoak, J., Reynolds, J., et al. 1990, MNRAS, 244, 130
Harris, W. E. 1991, ARA&A, 29, 543
Harris, W. E., & van den Bergh, S. 1981, AJ, 86, 1627
Harris, W. E., Harris, G. L., & Alessi, M. 2013, AJ, 772, 82
Harris, W. E., Ciccone, S. M., Eadie, G. M., et al. 2017, AJ, 835, 101
Hu, J. 2008, MNRAS, 386, 2242
Hughes, A. K., Sand, D. J., Seth, A., et al. 2021, ApJ, 914, 16
Jarrett, T., Chester, T., Cutri, R., et al. 2003, AJ, 125, 525
Jerjen, H., & Koribalski, B. S. 2008, Galaxies in the Local Volume (Springer), 41
Jones, K., Koribalski, B., Elmouttie, M., & Haynes, R. 1999, MNRAS, 302, 649
Koribalski, B. S., Staveley-Smith, L., Kilborn, V. A., et al. 2004, AJ, 128, 16
Lindegren, L., Hernández, J., Bombrun, A., et al. 2018, A&A, 616, A2
Marconi, A., Moorwood, A., Origlia, L., et al. 1994, The Messenger, 78, 20
Matt, G., Fiore, F., Perola, G., et al. 1996, MNRAS, 281, L69
Meyer, M. J., Zwaan, M. A., Webster, R. L., et al. 2004, MNRAS, 350, 1195
Minniti, D. 2018, The Vatican Observatory, Castel Gandolfo: 80th Anniversary Celebration (Springer), 63
Minniti, D., Alonso, M., Goudfrooij, P., et al. 1996, ApJ, 467, 221
Muratov, A. L., & Gnedin, O. Y. 2010, ApJ, 718, 1266
Nantais, J. B., & Huchra, J. P. 2010, AJ, 139, 2620
Nantais, J. B., Huchra, J. P., Barmby, P., Olsen, K. A., & Jarrett, T. H. 2006, AJ, 131, 1416
Obasi, C., Gómez, M., Minniti, D., & Alonso-García, J. 2021, A&A, 654, A39
Oliva, E., Salvati, M., Moorwood, A., & Marconi, A. 1994, A&A, 288, 457
Oliva, E., Marconi, A., Cimatti, A., & di Serego Alighieri, S. 1998, A&A, 329, L21
Rejkuba, M. 2001, A&A, 369, 812
Rejkuba, M. 2004, A&A, 413, 903
Schlafly, E. F., & Finkbeiner, D. P. 2011, AJ, 737, 103
Taylor, M. A., Puzia, T. H., Gomez, M., & Woodley, K. A. 2015, AJ, 805, 65
van den Bergh, S., & Harris, W. E. 1982, AJ, 87, 494
Vasiliev, E. 2019, MNRAS, 484, 2832
Voggel, K. T., Seth, A. C., Sand, D. J., et al. 2020, ApJ, 899, 140
Wang, S., Ma, J., Wu, Z., et al. 2014, ApJ, 148, 4
Whiteoak, J. B., & Bunton, J. D. 1985, PASA, 6, 171
Woodley, K. A., & Gómez, M. 2010, PASA, 27, 379
Woodley, K. A., Harris, W. E., Puzia, T. H., et al. 2009, AJ, 708, 1335
Yamada, T., Takata, T., Djamaluddin, T., et al. 1993, ApJS, 89, 57
Yang, Y., Wilson, A. S., Matt, G., et al. 2009, ApJ, 691, 131

Appendix A: Colour cuts and list of GC candidates

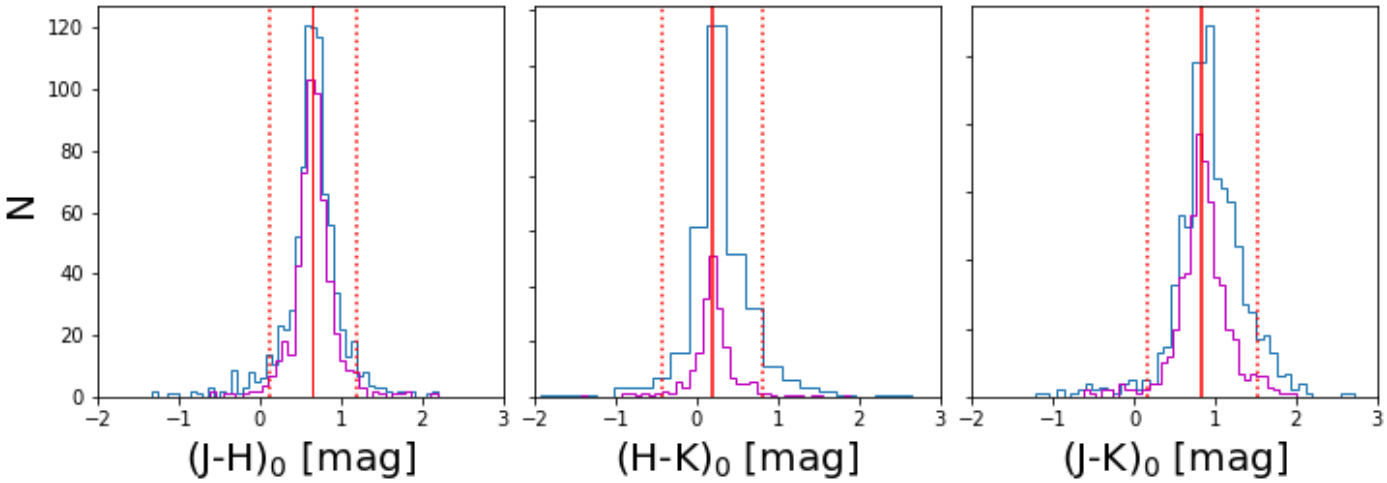

Fig. A.1. Two-sigma colour cuts (broken red vertical lines) with respect to the peak colour distribution of the confirmed GCs catalogue of Wang et al. (2014) in M31. The distribution of the confirmed Gcs in the catalogue is shown in magenta.

Table A.1. Near-IR VVVX photometry, colour, and shape parameters of our cluster candidates.

ID	RA DD	DEC DD	J mag	σJ mag	H mag	σH mag	K_s mag	σK_s mag	G mag	FWHM pixels	ε	A_V mag	A_J mag	A_H mag	A_{ks} mag	A_G mag	D kpc
0	209.646	-65.2543	16.55	0.02	16.29	0.04	16.28	0.08	17.28	3.81	0.26	2.14	0.6	0.39	0.25	1.84	106
1	209.9556	-65.7977	16.41	0.02	16.04	0.03	15.9	0.06	17.46	2.49	0.11	1.87	0.52	0.34	0.22	1.6	101
2	210.0543	-65.896	15.65	0.02	15.28	0.02	15.31	0.04	16.57	3.11	0.1	1.82	0.51	0.34	0.22	1.57	101
3	210.702	-65.2801	17.23	0.03	16.91	0.06	16.91	0.1	18.28	2.64	0.21	2.34	0.66	0.43	0.28	2.02	76
4	210.8203	-65.5881	17.16	0.02	16.56	0.04	16.4	0.07	19.18	2.97	0.18	1.77	0.49	0.32	0.21	1.52	74
5	211.1837	-65.2004	15.03	0.01	14.78	0.01	14.74	0.02	15.72	3.16	0.09	2.17	0.61	0.4	0.26	1.86	62
6	211.1937	-65.1237	16.37	0.02	16.01	0.03	16.09	0.06	17.42	3.66	0.24	2.16	0.6	0.4	0.25	1.85	63
7	211.5559	-65.7712	15.76	0.01	15.24	0.01	15.17	0.02	17.22	2.67	0.05	1.47	0.41	0.27	0.17	1.27	59
8	211.9328	-65.6819	15.72	0.01	15.47	0.01	15.46	0.02	16.53	2.61	0.08	1.58	0.44	0.29	0.19	1.36	46
9	212.7034	-65.4799	16.05	0.01	15.68	0.02	15.56	0.04	17.1	3.5	0.3	1.77	0.5	0.33	0.21	1.52	20
10	209.6601	-65.1488	15.73	0.01	15.52	0.02	15.5	0.04	16.14	3.01	0.18	2.52	0.71	0.46	0.3	2.17	107
11	209.9389	-65.7813	16.03	0.02	15.79	0.02	15.86	0.05	16.75	3.74	0.09	1.89	0.53	0.35	0.22	1.62	102
12	211.0332	-65.9285	16.26	0.01	15.87	0.02	15.73	0.05	17.42	3.68	0.16	1.34	0.38	0.25	0.16	1.15	77
13	210.2055	-65.0511	15.44	0.01	15.16	0.02	15.12	0.04	15.89	2.98	0.04	2.98	0.83	0.55	0.35	2.56	93
14	211.058	-64.9099	16.42	0.02	15.82	0.03	15.86	0.04	17.19	3.87	0.15	2.13	0.6	0.39	0.25	1.83	72
15	210.0427	-65.1478	15.85	0.01	15.4	0.02	15.37	0.03	17.24	2.8	0.14	2.48	0.69	0.46	0.29	2.13	96
16	209.8827	-65.3385	15.14	0.01	14.92	0.01	14.95	0.03	15.81	2.81	0.1	1.89	0.53	0.35	0.22	1.62	99
17	210.1386	-65.6147	16.46	0.03	16.0	0.04	16.02	0.08	17.92	3.15	0.03	1.77	0.5	0.33	0.21	1.52	93
18	210.6621	-64.9864	15.59	0.01	15.23	0.01	15.27	0.03	16.03	2.87	0.12	2.79	0.78	0.51	0.33	2.4	81
19	210.9808	-65.0815	15.6	0.01	15.29	0.02	15.28	0.03	16.34	3.21	0.13	2.38	0.67	0.44	0.28	2.04	70
20	210.8899	-65.2929	15.44	0.02	15.14	0.02	15.19	0.03	16.38	3.12	0.02	2.15	0.6	0.4	0.25	1.85	70
21	211.0256	-65.3646	15.85	0.02	15.58	0.02	15.53	0.04	16.6	4.0	0.32	2.04	0.57	0.38	0.24	1.76	66
22	211.2093	-65.5939	16.56	0.02	16.25	0.03	16.22	0.06	17.58	3.27	0.08	1.63	0.46	0.3	0.19	1.4	63
23	211.3385	-65.5525	15.5	0.02	15.17	0.02	15.16	0.03	16.27	3.99	0.21	1.66	0.46	0.31	0.2	1.43	59
24	211.9026	-65.095	15.58	0.02	15.22	0.02	15.38	0.03	16.45	3.6	0.23	1.96	0.55	0.36	0.23	1.68	44
25	212.1071	-65.4834	16.24	0.02	15.89	0.02	15.89	0.05	17.03	3.18	0.21	1.6	0.45	0.29	0.19	1.37	36
26	212.6931	-65.103	16.18	0.01	15.79	0.02	15.76	0.05	17.12	3.26	0.29	2.18	0.61	0.4	0.26	1.87	24
27	212.6585	-65.355	15.23	0.01	14.99	0.01	14.95	0.02	15.8	3.4	0.18	1.99	0.56	0.37	0.23	1.71	18
28	212.7143	-65.4207	16.24	0.01	15.73	0.02	15.59	0.04	17.77	2.74	0.21	1.84	0.52	0.34	0.22	1.58	18
29	212.6281	-65.2966	16.58	0.02	16.14	0.02	16.0	0.05	18.1	3.4	0.32	2.05	0.57	0.38	0.24	1.76	20
30	212.8148	-65.5737	16.59	0.02	16.2	0.03	16.15	0.06	17.84	2.98	0.12	1.63	0.46	0.3	0.19	1.4	21
31	211.0072	-65.0896	16.94	0.02	16.53	0.05	16.69	0.08	17.89	3.73	0.12	2.38	0.67	0.44	0.28	2.04	69
32	210.9581	-65.4085	16.61	0.02	15.99	0.03	16.04	0.06	18.22	3.56	0.14	1.99	0.56	0.37	0.23	1.71	68
33	211.7361	-65.0835	16.09	0.01	15.66	0.02	15.61	0.04	17.78	3.1	0.03	1.95	0.55	0.36	0.23	1.67	49
34	211.8109	-65.0526	16.31	0.02	15.93	0.03	15.94	0.04	17.53	3.46	0.17	2.0	0.56	0.37	0.24	1.72	48
35	211.7861	-65.3681	17.46	0.03	17.06	0.05	16.99	0.13	19.43	2.99	0.26	1.56	0.44	0.29	0.18	1.34	44

Table A.1. continued.

ID	RA DD	DEC DD	J mag	σJ mag	H mag	σH mag	K_s mag	σK_s mag	G mag	FWHM pixels	ε	A_V mag	A_J mag	A_H mag	A_{ks} mag	A_G mag	D kpc
36	212.0291	-65.3367	16.52	0.01	16.01	0.02	15.94	0.05	17.68	3.78	0.34	1.63	0.46	0.3	0.19	1.4	37
37	211.9312	-65.6224	15.1	0.01	14.79	0.01	14.75	0.02	16.02	2.99	0.18	1.64	0.46	0.3	0.19	1.41	44
38	212.553	-64.957	15.63	0.01	15.37	0.02	15.34	0.03	16.35	3.68	0.09	2.69	0.75	0.49	0.32	2.31	34
39	213.251	-65.7362	16.71	0.02	16.11	0.03	15.98	0.05	18.15	2.95	0.17	1.59	0.44	0.29	0.19	1.36	28
40	213.3396	-65.7953	17.55	0.04	17.21	0.06	16.88	0.13	19.48	3.0	0.2	1.61	0.45	0.3	0.19	1.39	32
41	212.9437	-65.2087	17.07	0.03	16.58	0.03	16.39	0.1	18.49	2.88	0.18	2.01	0.56	0.37	0.24	1.73	14
42	213.0214	-65.2235	15.46	0.01	15.21	0.01	15.21	0.03	16.01	3.5	0.37	2.05	0.57	0.38	0.24	1.76	11
43	213.1648	-65.1713	16.32	0.01	15.87	0.02	15.84	0.06	17.47	2.36	0.23	1.88	0.53	0.35	0.22	1.62	12
44	213.4063	-65.5202	16.73	0.02	16.4	0.02	16.3	0.07	18.05	3.6	0.08	1.63	0.46	0.3	0.19	1.4	13
45	213.6302	-65.7496	16.42	0.01	15.9	0.01	15.84	0.06	18.48	3.6	0.1	1.51	0.42	0.28	0.18	1.3	30
46	213.6953	-65.6493	17.2	0.03	16.83	0.05	16.67	0.1	19.0	3.01	0.25	1.5	0.42	0.28	0.18	1.29	25
47	213.9453	-64.84	16.76	0.02	16.24	0.02	16.17	0.07	17.99	3.1	0.13	2.85	0.8	0.52	0.34	2.45	40
48	214.2796	-65.4149	16.88	0.02	16.46	0.03	16.38	0.08	18.09	2.87	0.24	1.88	0.53	0.35	0.22	1.61	29
49	214.5096	-64.6824	16.9	0.02	16.38	0.02	16.64	0.08	18.02	3.85	0.13	2.56	0.72	0.47	0.3	2.2	58
50	214.7067	-64.7219	16.38	0.02	16.0	0.02	16.01	0.06	17.5	2.47	0.02	2.54	0.71	0.47	0.3	2.18	60
51	214.6406	-64.5995	16.14	0.01	15.88	0.02	15.95	0.05	16.86	3.96	0.36	2.49	0.7	0.46	0.29	2.14	65
52	214.7177	-64.8725	16.78	0.03	16.47	0.03	16.56	0.1	17.63	2.92	0.22	2.68	0.75	0.49	0.32	2.3	53
53	214.9468	-64.8944	16.39	0.03	16.0	0.03	15.91	0.06	17.6	2.42	0.16	2.78	0.78	0.51	0.33	2.39	58
54	215.0736	-65.0166	15.21	0.01	15.0	0.01	14.98	0.03	15.78	2.51	0.28	2.69	0.75	0.49	0.32	2.31	57
55	214.9383	-65.2082	15.02	0.01	14.8	0.01	14.8	0.02	15.54	2.31	0.05	2.13	0.6	0.39	0.25	1.83	49
56	215.42	-65.4863	16.08	0.01	15.83	0.02	15.72	0.04	16.92	3.25	0.24	1.68	0.47	0.31	0.2	1.44	63
57	215.261	-64.5335	17.09	0.03	16.53	0.03	16.44	0.08	18.32	3.02	0.2	2.69	0.75	0.5	0.32	2.32	81
58	213.3722	-65.621	15.56	0.01	15.31	0.02	15.24	0.03	16.25	3.63	0.21	1.58	0.44	0.29	0.19	1.36	20
59	215.677	-64.7121	15.17	0.02	14.98	0.03	15.0	0.03	16.03	2.67	0.08	2.75	0.77	0.51	0.32	2.37	83
60	214.187	-64.497	15.95	0.01	15.68	0.02	15.76	0.05	16.46	2.5	0.17	2.96	0.83	0.54	0.35	2.55	64
61	214.4463	-64.888	16.27	0.01	15.82	0.02	15.8	0.04	17.4	3.52	0.36	2.57	0.72	0.47	0.3	2.21	46
62	214.6598	-65.1219	16.12	0.01	15.8	0.02	15.76	0.04	16.93	2.38	0.09	2.3	0.64	0.42	0.27	1.98	43
63	214.676	-65.1239	16.17	0.02	15.69	0.02	15.42	0.06	17.25	3.68	0.39	2.3	0.64	0.42	0.27	1.98	43
64	214.9766	-64.3485	15.03	0.02	14.91	0.02	14.86	0.03	15.38	2.77	0.23	2.85	0.8	0.52	0.34	2.45	85
65	215.9346	-64.6718	16.63	0.02	16.09	0.02	15.95	0.04	18.11	3.96	0.3	2.41	0.67	0.44	0.28	2.07	91
66	215.9726	-64.5859	15.02	0.01	14.9	0.01	14.86	0.02	15.24	2.93	0.22	2.36	0.66	0.43	0.28	2.03	95
67	216.1489	-64.9173	17.68	0.05	17.4	0.07	17.19	0.15	18.85	3.44	0.05	1.9	0.53	0.35	0.22	1.63	89
68	213.6556	-65.0388	16.91	0.02	16.46	0.03	16.17	0.08	17.81	3.02	0.2	2.33	0.65	0.43	0.27	2.0	24
69	214.9895	-65.5057	16.78	0.02	16.34	0.02	16.19	0.06	17.85	2.91	0.17	1.76	0.49	0.32	0.21	1.51	51
70	214.9922	-64.8638	16.82	0.02	16.54	0.03	16.56	0.09	17.55	2.32	0.24	2.73	0.77	0.5	0.32	2.35	60
71	215.2915	-65.1353	16.8	0.02	16.48	0.02	16.55	0.08	17.52	3.71	0.25	2.14	0.6	0.39	0.25	1.84	60
72	215.554	-65.0999	15.74	0.01	15.44	0.02	15.4	0.03	16.53	2.33	0.03	2.1	0.59	0.39	0.25	1.8	68
73	215.7254	-64.4617	16.35	0.02	15.98	0.02	16.05	0.06	17.16	2.5	0.18	2.58	0.72	0.48	0.3	2.22	95
74	216.3452	-65.0076	16.21	0.01	15.82	0.01	15.66	0.04	17.3	3.22	0.3	1.7	0.48	0.31	0.2	1.46	92
75	215.7889	-65.4676	17.89	0.03	17.19	0.03	16.78	0.11	19.73	2.66	0.07	1.42	0.4	0.26	0.17	1.22	73
76	215.8472	-65.4723	15.94	0.01	15.61	0.01	15.41	0.03	16.95	3.58	0.34	1.39	0.39	0.26	0.16	1.19	75
77	214.4796	-65.3112	15.08	0.04	14.89	0.05	14.53	0.03	15.66	2.77	0.04	2.01	0.56	0.37	0.24	1.73	35